Raman Study of Pure and Semiconducting CdF_2. The Polaron Problem

P. EISENBERGER
Bell Telephone Laboratories, Murray Hill, New Jersey 07974

AND

M. G. ADLERSTEIN*
Division of Engineering and Applied Physics, Harvard University, Cambridge, Massachusetts 02138

(Received 16 June 1969)

The technique of Raman spectroscopy is employed to investigate pure and semiconducting CdF_2. The results in the pure material are used together with previously reported optical data to calculate, within the framework of the rigid-ion model, the phonon dispersion relations and density of states of pure CdF_2. The dispersion relations cannot be obtained experimentally because of the large neutron-capture cross section of cadmium. In semiconducting CdF_2, two new Raman peaks are observed. One of them is interpreted, through a Green's-function calculation, as being due to a local vibrational mode associated with the presence of the semiconducting electron. The accompanying lattice distortion is related via a small polaron model to the polaron mass; we obtain a value of 18 for the ratio of polaron mass to band mass. Ultraviolet reflection data on pure CdF_2 are presented and interpreted in terms of a hydrogenic exciton model which predicts a band mass of $0.8m_e$. These results, taken together with the measured cyclotron mass $11m_e$, suggest that neither large- nor small-polaron models are appropriate to describe the CdF_2 polaron, but that an intermediate-polaron model is necessary.

I. INTRODUCTION

THE purpose of this paper is twofold. First, it is to present a calculation of the phonon dispersion relations and density of states for pure CdF_2 based on a rigid-ion model and, second, to further illuminate the nature of the electron-phonon interaction responsible for mass enhancement of the conduction electron in semiconducting (SC) CdF_2.

In Sec. II we present the Raman spectrum of pure CdF_2 and interpret the peaks in terms of the $\mathbf{q}\cong 0$ Raman-active phonon modes and two-phonon sum and difference modes. The energy, 322 cm^{-1}, of the T_{2g} mode together with previously measured[1,2] energies of the infrared-active $\mathbf{q}\cong 0$ modes are used to deduce that the force constants in CdF_2 are identical to those in CaF_2 to within 1%. Since force constants in CaF_2 are known one can calculate the phonon dispersion relations and density of states of CdF_2. These results are particularly useful since the high neutron-capture cross section of cadmium makes their experimental determination impractical.

Physically, SC CdF_2 differs from pure CdF_2 in that one has introduced, by chemical treatment,[3] mobile electrons which can reside in donorlike traps. The traps are believed to be describable as electrons localized about trivalent rare-earth impurities introduced substitutionally for the divalent Cd ions. A typical impurity concentration is 0.05%. Several properties of SC CdF_2 have been determined by previous experiments[3–8] and it is believed that at sufficiently low frequencies, conduction processes must involve polarons to some degree. A cyclotron mass at 12.5 Gc/sec of $11m_e$ has been measured.[5] Little is known, however, about the exact nature of the electron-phonon coupling in CdF_2 which produces the large mass enhancement.

The cause of this difficulty arises from uncertainties about the size of the polaron in CdF_2. Large-polaron calculations made in conjunction with the measured polaron mass of $11m_e$ give a value of 5.8 Å for the radius of the polaron. This is the same size as the unit cell in CdF_2 and thus the validity of the Fröhlich Hamiltonian and large-polaron picture is in doubt. As the lattice distortion around the conduction electrons becomes more localized (i.e., small polaron), one might expect that the detailed dynamics of the lattice become important and that local modes may be produced. It was the original purpose of this study to see if the effects of the electron's presence on the lattice could be observed and thus the size of the polaron evaluated.

Two new Raman transitions are observed in SC CdF_2 which are not observed in either the pure and doped insulating state of CdF_2. Their properties are discussed in Sec. III.

There is an A_{1g} symmetry transition at 262 cm^{-1} which can be attributed to a local phonon mode induced in the lattice by the presence of the mobile electrons. The conduction band in CdF_2 is composed of Cd^{+2} $5s$ atomiclike states[5,6] so that conduction electrons reside on Cd^{+2} ions. The same is true of the trap states which

* Supported in part by the Joint Services Electronic Program (U. S. Army, U. S. Navy, and U. S. Air Force) under Contract No. Nonr-1866(16), and by the Division of Engineering and Applied Physics, Harvard University.

[1] D. R. Bosomworth, Phys. Rev. **157**, 709 (1967).

[2] J. D. Axe, J. W. Gaglianello, and J. E. Scordefield, Phys. Rev. **139**, A1211 (1965).

[3] J. D. Kingsley and J. S. Prenner, J. Chem. Phys. **38**, 667 (1963).

[4] P. Eisenberger and P. S. Pershan, Phys. Rev. **167**, 292 (1968).

[5] P. Eisenberger, P. S. Pershan, and D. R. Bosomworth, Phys. Rev. Letters **21**, 543 (1968).

[6] P. Eisenberger, P. S. Pershan, and D. R. Bosomworth, Phys. Rev. (to be published).

[7] P. F. Weller, Inorg. Chem. **4**, 1545 (1965).

[8] P. Eisenberger and P. S. Pershan, Appl. Phys. Letters **10**, 248 (1967).

are split off from the conduction band by their proximity to the rare earth. The trapped electron in its ground state is thought to hop among the 12 nearest-neighbor Cd^{+2} sites. The presence of an electron at a Cd^{+2} site will polarize the surrounding medium (e.g., the neighboring fluorines move away). The accompanying change in the local force constant can result in a local phonon mode provided there is a gap in the density of states. A Green's-function calculation, using the results to be presented in Sec. II, of the local A_{1g} density of states indeed shows such a gap around 260 cm^{-1}.

A second A_{1g} symmetry transition at 180 cm^{-1} will be attributed to electronic levels forming the electron traps. An infrared absorption peak observed at 178 cm^{-1} in SC CdF_2 [5,6] has already been explained in terms of such levels. The relationship between these results is discussed in Sec. III.

In Sec. IV we present an impurity Green's-function calculation to determine the perturbation in the effective local force constants necessary to produce a local mode at 262 cm^{-1}.

In Sec. V we use a small-polaron theory to derive an expression for the ratio of the polaron mass to the band mass in terms of the above-mentioned perturbation.

In Sec. VI, uv reflection data taken on pure CdF_2 between 4 and 19 eV are briefly presented. The results are interpreted in terms of excitonic and interband transitions; an excitonic mass of $0.8m_e$ is obtained. The hydrogenic model of the exciton used in our case is identical to that applied to the uv spectrum of pure CaF_2 where the model predicts an exciton mass of $0.27m_e$. These results support the view[5,6] that the large electron affinity of atomic Cd not only lowers the band gap of CdF_2 relative to that of CaF_2 but also is responsible for the larger conduction band mass in CdF_2.

In Sec. VII, the present state of the polaron model for CdF_2 is discussed and critically evaluated.

II. RAMAN STUDY OF PURE CdF_2

We have measured the Raman spectrum of pure CdF_2 with an argon laser and our results are shown in Fig. 1. The strong line at 322 cm^{-1} arises from purely off-diagonal Raman tensor components, which means, in a crystal of O_h point group symmetry, that the mode producing it has T_{2g} symmetry. The weak structures at other frequencies are two-phonon Raman peaks which will be discussed in the Appendix.

CdF_2 has the fluorite structure with a lattice parameter of 5.40 Å. Because there are three atoms per unit cell, there is a total of nine phonon branches, three acoustic and six optic. At $\mathbf{q}\cong 0$, three of the optic branches have T_{1u} symmetry: the longitudinal and transverse infrared modes; three have T_{2g} symmetry: the longitudinal and transverse Raman modes. The presence of long-range Coulomb forces causes the transverse and longitudinal infrared modes to be nondegenerate at finite $\mathbf{q}$. The strong line at 322 cm^{-1} can be identified with the T_{2g} $\mathbf{q}\cong 0$ Raman mode of CdF_2.

Much work has been done on the infrared properties of CdF_2 by Bosomworth[1] and Axe *et al.*[2] The optical parameters found by their experiments are shown in

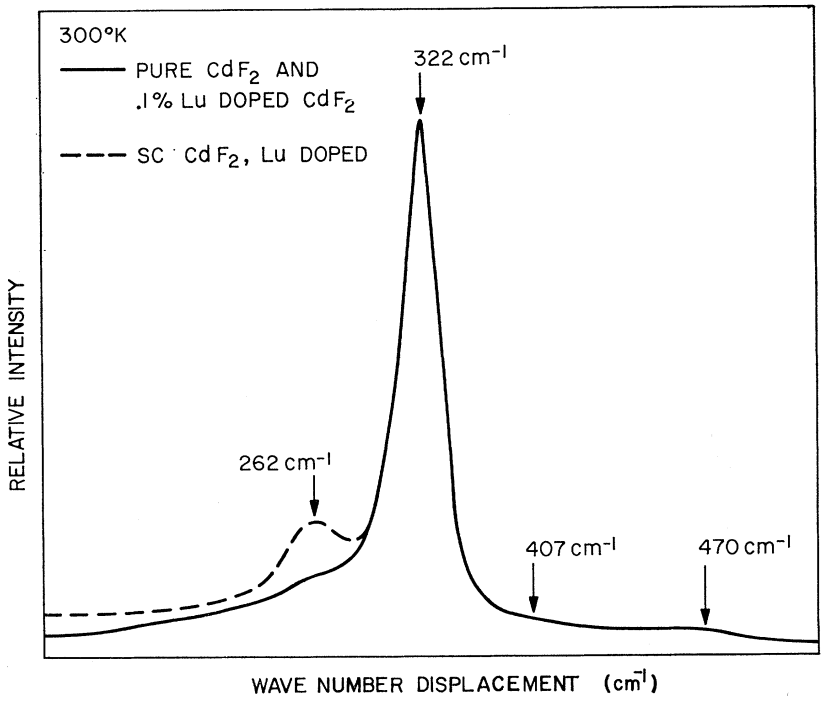

FIG. 1. Raman spectrum of pure CdF_2—both diagonal and off-diagonal components of the Raman tensor can contribute.

Table I. Also listed in Table I are the corresponding parameters for CaF_2. CaF_2 also has the fluorite structure with a lattice parameter of 5.45 Å and exhibits a T_{2g} $\mathbf{q}\cong 0$ Raman mode also at 322 cm^{-1}. There is no dipole moment associated with this Raman vibration in the fluorite structure and there is no motion of the positive ion. The equivalence of the T_{2g} Raman frequencies indicates that the short-range force constants involved are the same in the two systems and suggests that the phonon dispersion relations of CdF_2 can be generated from those of CaF_2 if one simply changes the mass used in the analysis from that of Ca to that of Cd.

The correctness of this approach may be further substantiated if one examines the rigid-ion-model expression for the transverse optic frequency[9]:

$$\omega_{TO}^2=-\frac{m_1+2m_2}{m_1m_2}\left[R_{12}-\frac{4\pi e^2}{9V}(Z_1'Z_2')\right], \quad (1)$$

where R_{12} is the metal (1)–fluorine (2) short-range repulsive force constant and Z_1' and Z_2' are the effective charges of the metal ion and fluorine ion, respectively, and where V is the volume of the unit cell. Assuming only a mass change between CaF_2 and CdF_2, one obtains from Eq. (1)

$$\frac{\omega_{TO}^{CaF_2}}{\omega_{TO}^{CdF_2}}=\frac{(2/m_{Ca}+1/m_F)^{1/2}}{(2/m_{Cd}+1/m_F)^{1/2}}=1.20, \quad (2)$$

while from Table I the experimental ratio was found to be 1.19. The good agreement supports the view that all the force constants and effective charges are very nearly identical in the two crystals. Thus the force constants listed by Ganesan and Sirvasan[9] should also apply for CdF_2.

Lacina[10] has performed a rigid-ion-model[9] calculation of the lattice dynamics of pure CaF_2. In this model the fluorite crystal is regarded as consisting of rigid, nonpolarizable ions interacting through long-range electrostatic and short-range repulsive forces. These forces are calculated from experimental knowledge of the $\mathbf{q}\cong 0$ Raman frequency ω_R, the longitudinal optical frequency ω_{LO}, the transverse optical frequency ω_{TO}, and the three elastic constants c_{11}, c_{12}, and c_{44}. The rigid-ion model for CaF_2 seems to be fairly successful not only because it can fit neutron-diffraction data[11] but also because $\mathbf{q}\cong 0$ shell-model calculations[12] in which electronic polarizability effects are explicitly included give results for the force constants which differ by less than 10% from those obtained from the rigid-ion model.[9]

TABLE I. Optical properties of CdF_2 and CaF_2.

Structure lattice parameter (Å)	CaF_2 Fluorite 5.45	CdF_2 Fluorite 5.40
ϵ_∞	2.04	2.4
ϵ_0 (300°K)	6.63	8.49
ϵ_0 (80°K)	6.38	7.78
ω_{TO}(80°K) (cm^{-1})	267	224
ω_{LO}(80°K) (cm^{-1})	472	403

Using experimental quantities known for CdF_2, but keeping the CaF_2 elastic constants, we have obtained dispersion curves in the ⟨100⟩, ⟨110⟩, and ⟨111⟩ directions as well as the total density of states for CdF_2 from the same model (Fig. 2). In Fig. 3 for comparison, are shown the results of Lacina for CaF_2. Due primarily to the greater Cd mass, the acoustic branch is considerably lower in frequency. The transverse and longitudinal optical branches are slightly lower in frequency. The Raman branch is essentially unaltered.

Because the rigid-ion model is only an approximation, and because of the assumed identity of the CdF_2 and CaF_2 force constants, we expect that the details of the

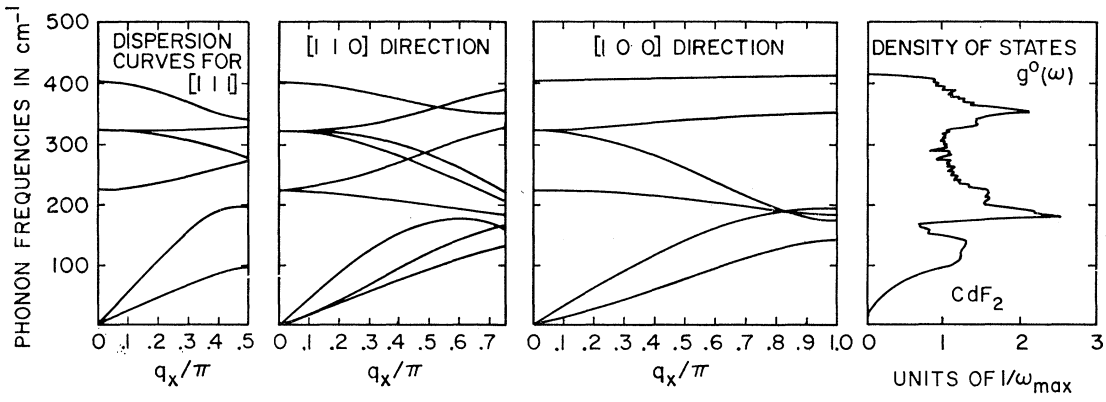

FIG. 2. Dispersion curves and density of states for CdF_2. The rigid-ion model is used.

[9] S. Genesan and R. Srinivasan, Can. J. Phys. **10**, 74 (1962).
[10] B. Lacina, thesis, Harvard University, 1969 (unpublished).
[11] P. Cribier, B. Farnoux, and B. Sacrot, Phys. Letters **1**, 187 (1962).
[12] J. D. Axe, Phys. Rev. **139**, 215 (1965).

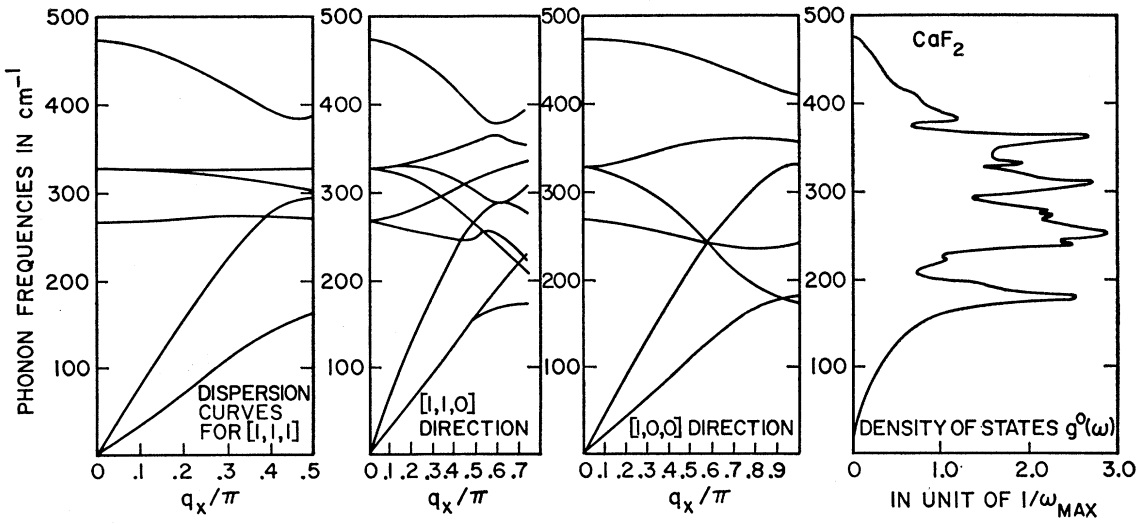

FIG. 3. Dispersion curves and density of states for CaF_2. The rigid-ion model is used (Ref. 10).

calculated dispersion curves are subject to uncertainty. However, average lattice properties of CdF_2 such as the density of states should be quite accurately given by the above approach.

The phonon calculation leads also to densities of states for arbitrary submodes of the pure lattice. In Fig. 4 is shown the frequency distribution for the A_{1g} symmetry breathing mode of a CdF_8 complex imbedded in the lattice in which the eight fluorines move in phase along the line joining them to the central Cd ion. The gap in the A_{1g} density of states in the 260-cm^{-1} region will prove very useful in understanding the Raman results in SC CdF_2. The procedure used in calculating both the density of states shown in Fig. 2 and the A_{1g} density of states shown in Fig. 4 are discussed full in Sec. IV.

III. RAMAN SPECTRUM OF SC CdF_2

No new signals were observed in doped but unconverted (insulating) CdF_2 for the dopant concentrations of 0.01–0.1% used here.

Upon conversion to SC CdF_2,[3] two new peaks were observed. For each of the samples doped with ytterbium, gadolinium, lutetium, or neodymium, the corresponding peaks occurred at the same energies and had

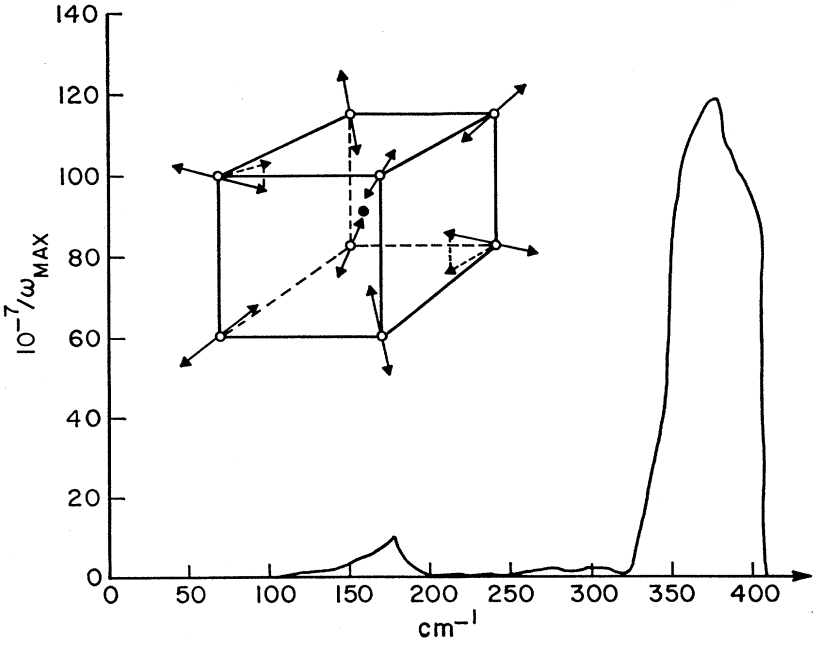

FIG. 4. Density of states in CdF_2 of $Cd^{++}F_8$ A_{1g} breathing mode.

identical characteristics. However, the two peaks were considerably different and will be discussed separately.

That which occurred at 180 cm^{-1} was observed only below 100°K. It is shown in Fig. 5. Its symmetry was unambiguously determined to be A_{1g} by polarization studies in which ⟨100⟩ and ⟨110⟩ crystal orientations were employed. Its temperature dependence, shown in Fig. 6, is completely different from what one would expect from absorption or population considerations for a phonon transition. As the temperature is elevated, the line disappears, at least partially, by broadening. The background radiation makes quantitative linewidth studies difficult, but the linewidth between 35 and 77°K was estimated to increase by about a factor of 2. There was no change between 4 and 35°K.

The frequency of the 180-cm^{-1} Raman peak is very close to that of the observed peak in the far-infrared absorption spectrum of SC CdF_2. This spectrum is shown in Fig. 7. Though the absorption peak has a somewhat smaller linewidth, neither it nor the Raman peak show any linewidth variation below 35°K.

The evidence suggests that the two lines result from essentially the same transition even though the symmetries are different. The 178-cm^{-1} absorption line has been previously identified as arising from an intratrap electronic transition between the A_{1g} ground state and a T_{1u} excited state.[5,6] The appearance of a similar transition in the Raman spectrum must involve a perturbation which ruins the pure symmetries of the states. One possible explanation is that electron-phonon coupling mixes in odd-parity phonon states into the excited state by $\mathbf{q}\cong 0$ strain effects which gives the resulting transition A_1 character without a significant shift in its frequency. An alternative explanation involves the intertrap coupling which is thought to be responsible for the impurity band conductivity,[7] the broad background absorption observed in the far infrared[6] (see Fig. 7), and the observed electron spin resonance exchange phenomena.[4] Such coupling could, of course, destroy the pure symmetry of the transition and introduce A_1-like transitions at essentially the same frequency as the T_1 transition.

The latter explanation is also consistent with the observed temperature dependence of the Raman peak since thermally activated intertrap hopping of the electron could result in lifetime broadening. The coincidence of the rise in the infrared absorption at 30°K and the onset of broadening of the Raman line at 35°K lends additional support to the model presented above.

The second, and most significant, new transition detected in SC CdF_2 was at 262 cm^{-1} and was observable at all temperatures; it had A_{1g} symmetry. The mixed

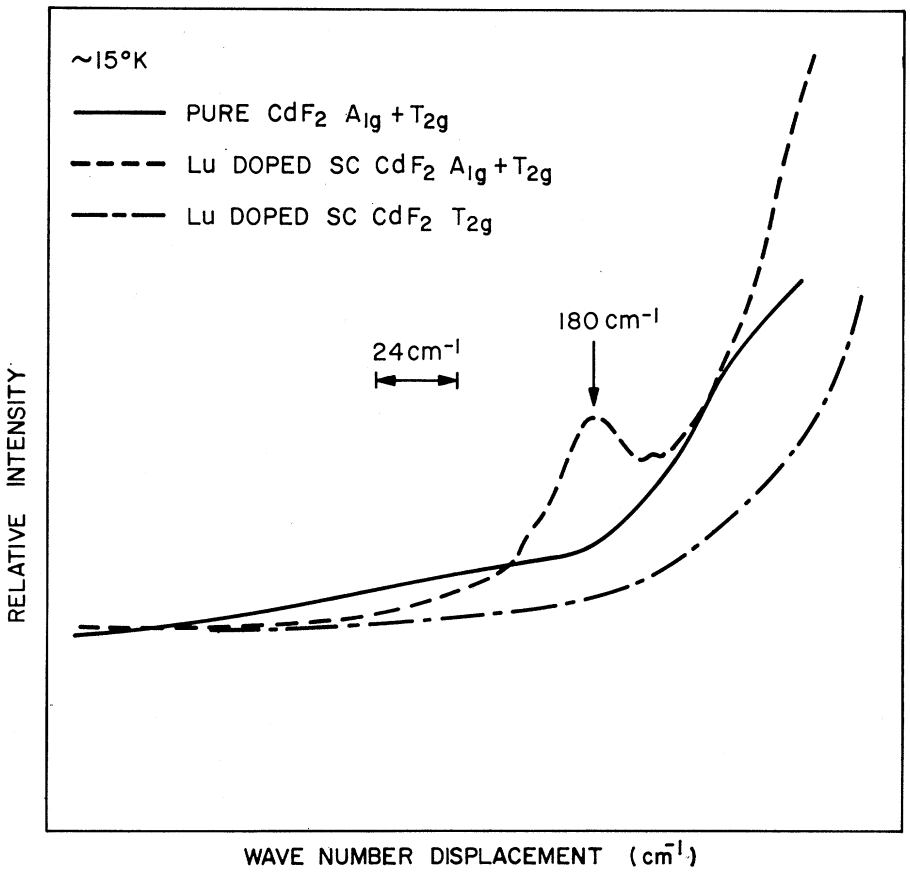

FIG. 5. The 180-cm^{-1} transition in SC CdF_2. Note its absence in pure CdF_2. When only off-diagonal components of the Raman tensor contribute it is also absent in SC CdF_2.

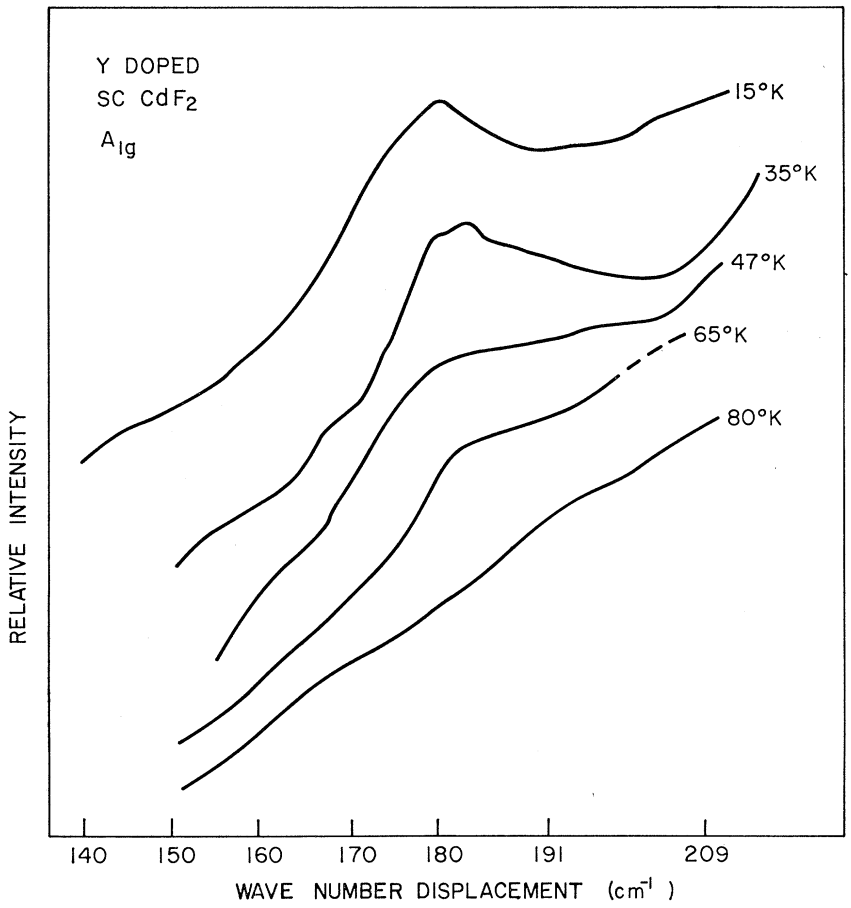

FIG. 6. Temperature dependence of 180-cm^{-1} transition.

polarization spectrum is given in Fig. 8 and a symmetry decomposition is given in Fig. 9. The intensity of the 262-cm^{-1} line relative to the allowed Raman line was a strong function of the frequency of excitation as shown in Fig. 10. This effect may be understood in terms of differences between the near-infrared absorption spectra of insulating versus semiconducting CdF_2. These spectra are given in Fig. 7. The absorption in the semiconductor has been attributed to excitations from low-lying donorlike states and it has a tail extending into the visible. Thus, as the Raman excitation frequency moves to regions of higher optical absorption, enhancement of the Raman peak may be occurring due to improved coupling between the electron and the light as observed in the Raman effect of F centers.[13,14]

This interpretation is consistent with temperature dependence of the line at 262 cm^{-1} as shown in Fig. 11. The signal is unnormalized. With decreasing temperature, it increases initially, peaks, decreases until 77°K and is then of constant intensity. In the same temperature region, the T_{2g} symmetry Raman signal at 322 cm^{-1} increased in intensity by about a factor of 4 with decreasing temperature between 300 and 77°K and was constant from 77 to 15°K. The behavior of both lines can be explained in terms of the decreasing optical absorption of the sample with decreasing temperature between 300 and 77°K as can be seen by considering the dependence of the two signals on the intensity of absorbed and transmitted laser power

$$I_{322}\sim I_{\text{transmitted}},\qquad I_{262}\sim\alpha_c I_{\text{transmitted}}. \tag{3}$$

Here, α_c is a measure of the coupling of the light to the semiconducting electrons via the tail of absorption associated with those electrons: α_c is proportional to I_{absorbed}. Thus the intensity of 262-cm^{-1} Raman transition varies in some sense as the product of the transmitted and absorbed laser power.

In the samples used in this experiment, the absorption coefficient at 5000 Å was about 4 cm^{-1} at room temperature and 1 cm^{-1} at 77°K and also 1 cm^{-1} at 4°K. Thus as the temperature is lower and the absorption decreases, the intensity of 322-cm^{-1} transition increases until the absorption becomes a constant below 77°K.[7] The 262-cm^{-1} line, on the other hand, initially goes through a maximum since $I_{\text{absorbed}}I_{\text{transmitted}}$ does, and

[13] J. M. Worlock and S. P. S. Porto, Phys. Rev. Letters **15**, 697 (1965).
[14] C. Henry, Phys. Rev. **152**, 699 (1966).

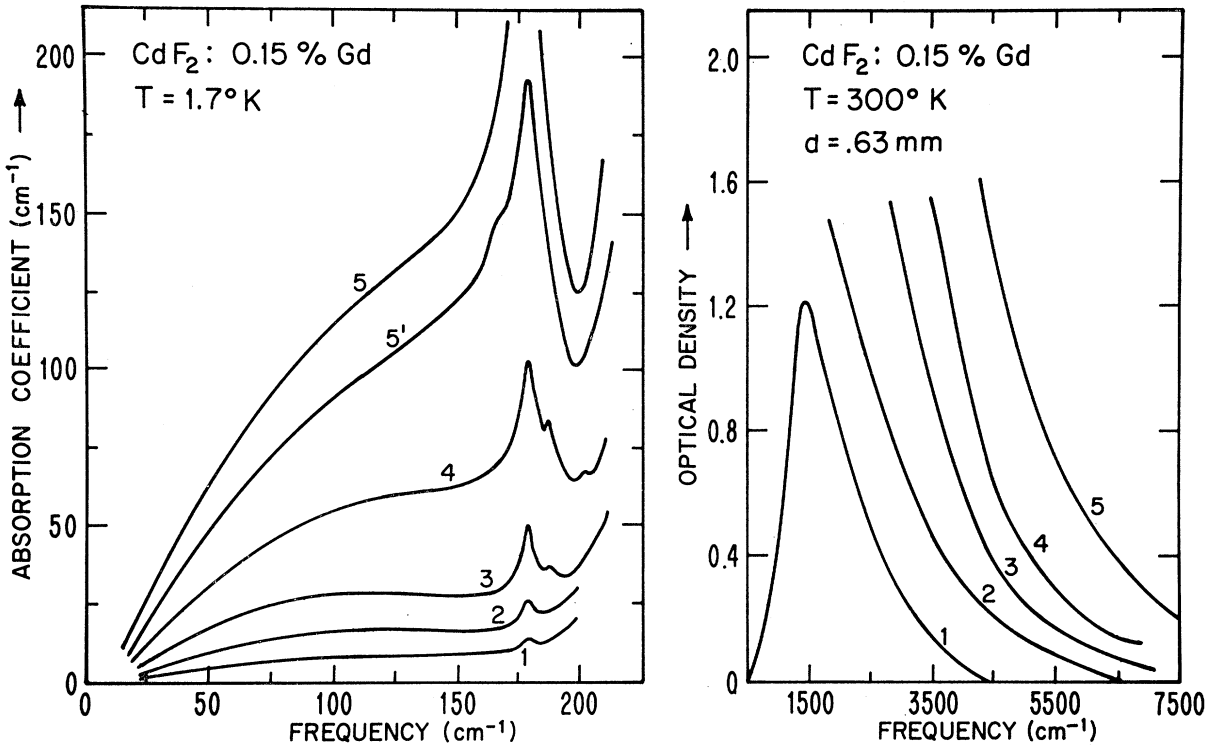

FIG. 7. Optical spectrum of SC CdF_2. Insulating CdF_2 has no absorption in the regions shown except its reststrahlen absorption band which extends from 200 to 650 cm^{-1}. Samples 1–5 differed in electron concentration from $4\times10^{16}/cm^3$ of sample 1 to $8\times10^{17}/cm^3$ of sample 5. The variation of absorption intensity was linear with electron concentration.

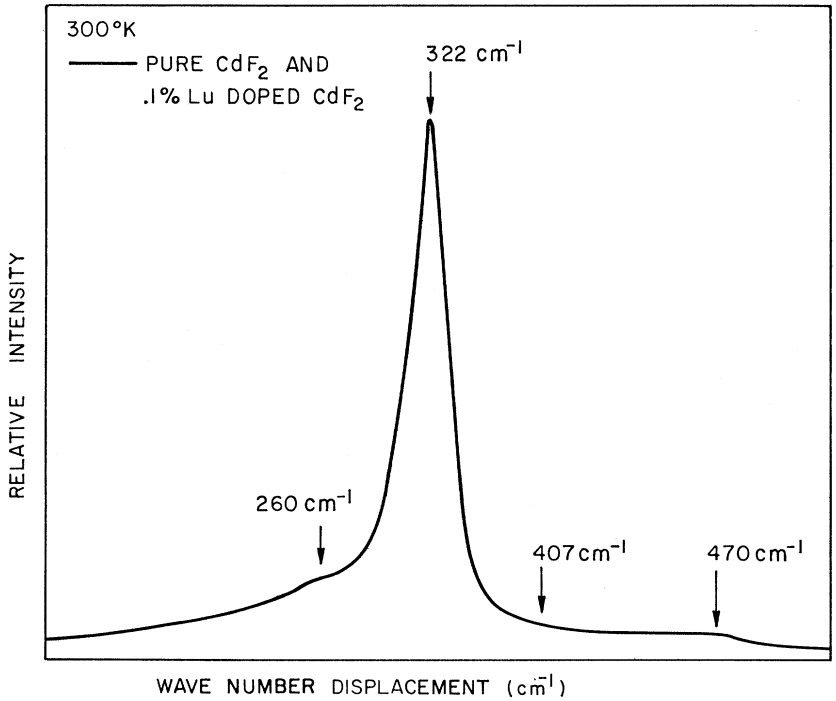

FIG. 8. Raman spectrum of SC CdF_2. Both diagonal and off-diagonal components can contribute to the spectrum.

then decreases as $I_{absorbed}$ continues to decrease. At 77°K, it too becomes constant. Any connection of the 262-cm^{-1} line with the two-phonon difference peak seen in the pure crystal around 262 cm^{-1} is ruled out by the failure of the 262-cm^{-1} line in SC CdF_2 to vanish at low temperatures. That this failure to vanish was not due

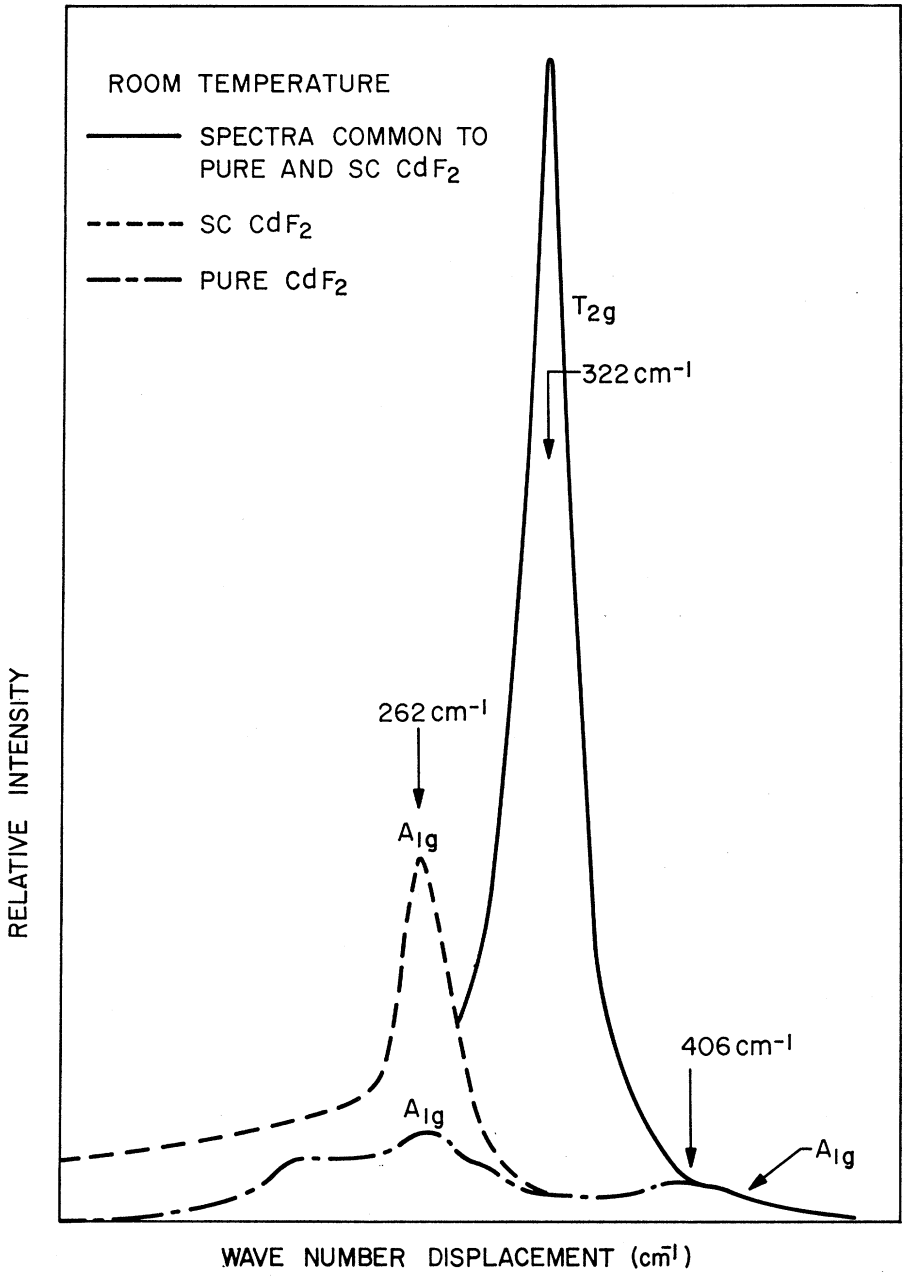

FIG. 9. Comparison of spectra of SC CdF_2 and pure CdF_2. Signals have been normalized to the 322-cm^{-1} Raman line and decomposed into their symmetry components.

to a heating effect was proven by a series of runs with different laser power in which the exact same temperature dependence was observed. The true second-order peaks behaved exactly like the 322-cm^{-1} Raman line.

The line shape at low temperatures seems to be broader than at higher temperatures. This can either be a real effect possibly due to the donor impurities as the electron becomes localized near them, or only an apparent increase caused by the presence of the two-phonon sum peak observed at 280 cm^{-1} in pure CdF_2.

The gap around 260 cm^{-1} in the A_{1g} density of states shown in Fig. 4 is such a strong feature that the identification of the 262-cm^{-1} line as a local mode seems very plausible. An obvious cause of such a local mode is evident from the following physical picture: If one places an electron at a Cd^{++} site one would expect the 8 nearest-neighbor fluorines (Fig. 12) to move away. As will be shown in Sec. V, this results in a decreased cadmium-fluorine repulsive force constant. This decreased force constant can be shown to shift the peak of the A_{1g} density of states from 380 cm^{-1} (Fig. 4) in pure CdF_2 to 262 cm^{-1} in SC CdF_2. The peak is also considerably sharpened. In Sec. IV we will calculate this effect by Green's-function techniques and the

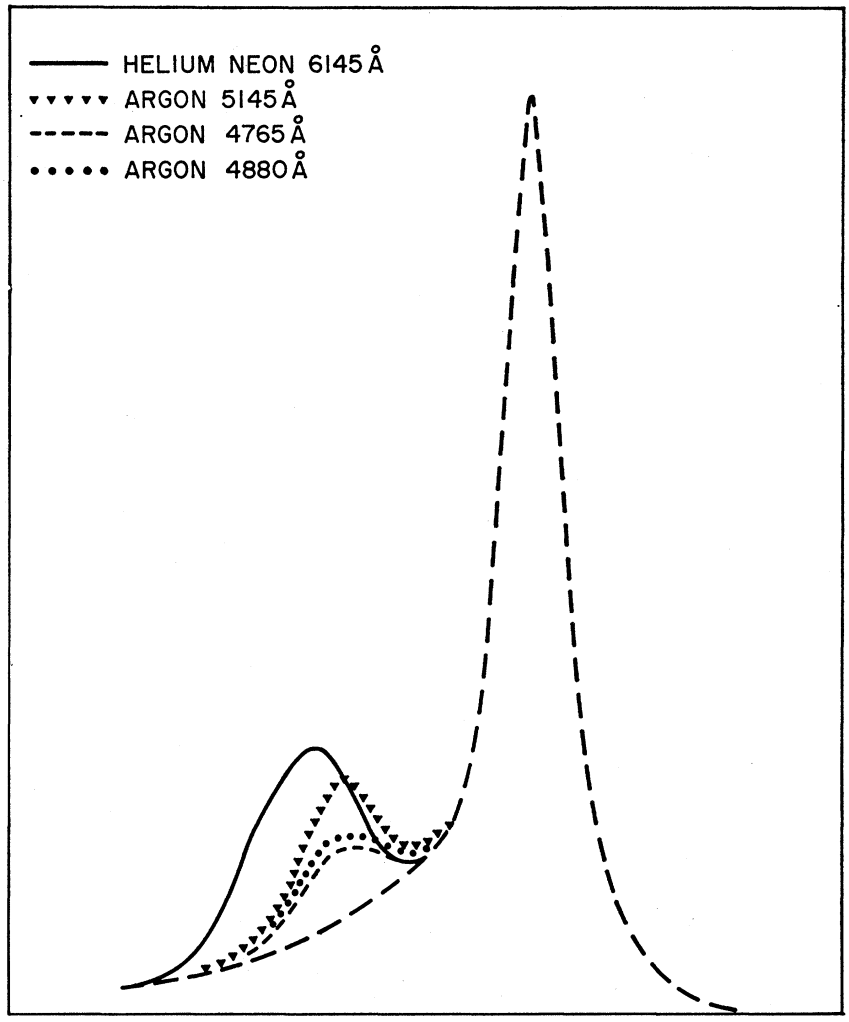

FIG. 10. The relative intensity of the 262-cm^{-1} transition at various frequencies of laser excitation at 300°K. The intensity is normalized to that of the large peak on the right which is the allowed Raman transition. The 262-cm^{-1} peak only appears to be moving away from the allowed Raman peak since the x-axis scale is in Angstroms rather than cm^{-1}.

results will be used to evaluate a change in the force constants of CdF_8 complex. In Sec. V, a physical model will be presented which will relate in quantitative terms the calculated force constant change to a lattice displacement. This, in turn, will be related to the polaron problem in CdF_2.

IV. ELECTRON-INDUCED LOCAL MODE

We first formulate, briefly, the lattice problem in terms of vector space representations of the crystal states[15] and apply these representations to calculating the Green's function appropriate to the semiconductor problem.

In the harmonic approximation, the Hamiltonian describing the crystal is

$$H_0=\tfrac{1}{2}\sum_{\alpha\kappa} m_\kappa^{-1}p_\alpha(l\kappa|t)^2 + \tfrac{1}{2}\sum_{\alpha\kappa l,\alpha'\kappa' l'} \Phi_{\alpha\alpha'}(ll',\kappa\kappa')u_\alpha(l\kappa|t)u_{\alpha'}(l'\kappa'|t), \quad (4)$$

where $p_\alpha(l\kappa|t)$ and $u_\alpha(l\kappa|t)$ are the α-polarized components of momentum and displacement from equilibrium, respectively, of the κth ion in the basis of the lth unit cell. Thus, $\alpha=x, y, z$ and $l=1, \ldots, N$, while $\kappa=1, 2, 3$, corresponding to the Cd^{+2} and the two F^- ions, respectively. The $\Phi_{\alpha\alpha'}(ll',\kappa\kappa')$ are the constants expressing the net forces acting between the ions and their numerical values depend upon the model chosen to represent the forces. In the present case, we have employed the "rigid-ion" model described in Sec. II.

It is useful to introduce the $9N$-dimensional vector space $\{|\alpha\kappa l\rangle\}$ whose basis vectors transform among themselves under operations of the crystal symmetry

[15] See, for example, R. J. Elliott, in *Phonons in Perfect Lattices and in Lattices with Point Imperfections*, edited by R. W. H. Stevenson (Plenum Press, Inc., New York, 1966).

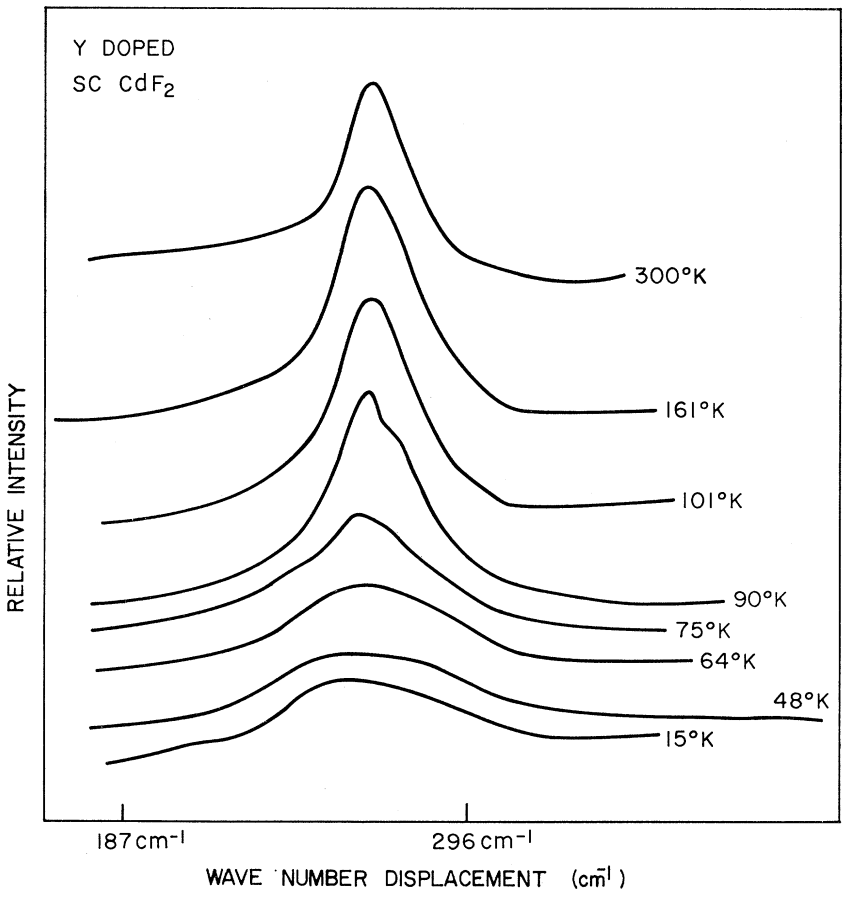

FIG. 11. Temperature dependence of 262-cm^{-1} line. The intensity is unnormalized.

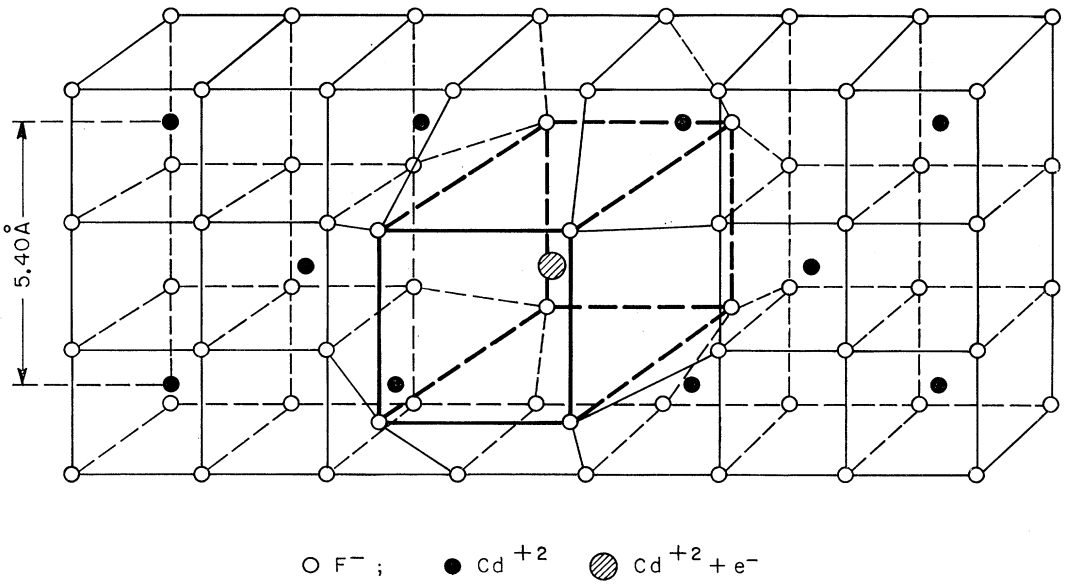

FIG. 12. Fluorite lattice showing polarization near Cd^{2+} site with semiconducting electron present. Fluorines move away from Cd site.

group as the correspondingly labeled ionic coordinates. The $|\alpha\kappa l\rangle$ are related to the physical state of the crystal by the equation

$$|u_\alpha(l,\kappa)\rangle = u_\alpha(l,\kappa)|\alpha\kappa l\rangle, \tag{5}$$

where $|u_\alpha(l,\kappa)\rangle$ is the crystal state where only the $(\alpha\kappa l)$ ionic displacement is nonzero and is $u_\alpha(l,\kappa)$. $\{|\alpha\kappa l\rangle\}$ is then a complete set.

From Eqs. (4) and (5) one finds the operator form of the dynamical equations to be

$$(\mathbf{M}\omega^2-\mathbf{\Phi})\sum_{\alpha\kappa l} u_\alpha(l,\kappa)|\alpha\kappa l\kappa = 0, \tag{6}$$

where $\mathbf{M}$ and $\mathbf{\Phi}$ are defined by their matrix elements

$$\begin{aligned}\langle\alpha\kappa l|\,\mathbf{M}\,|\alpha'\kappa' l'\rangle &= m_\kappa\delta_{\alpha\alpha'}\delta_{\kappa\kappa'}\delta_{ll'},\\ \langle\alpha\kappa l|\,\mathbf{\Phi}\,|\alpha'\kappa' l'\rangle &= \Phi_{\alpha\alpha'}(ll',\kappa\kappa').\end{aligned} \tag{7}$$

Equation (6) may be transformed to a convenient form by defining

$$\mathbf{D} = \mathbf{M}^{-1/2}\mathbf{\Phi}\mathbf{M}^{-1/2}, \tag{8}$$

where

$$\langle\alpha\kappa l|\,M^{\pm 1/2}\,|\alpha'\kappa' l'\rangle = m_\kappa^{\pm 1/2}\delta_{\alpha\alpha'}\delta_{\kappa\kappa'}\delta_{ll'},$$

in which case

$$(\omega^2\mathbf{1}-\mathbf{D})\sum_{\alpha\kappa l} u_\alpha(l,\kappa)m_\kappa^{1/2}|\alpha\kappa l\rangle = 0. \tag{9}$$

The translational periodicity of the lattice may be used to simplify Eq. (9). The eigenvectors of $(\omega^2\mathbf{1}-\mathbf{D})$ are the orthonormal phonon states $|\mathbf{q},j\rangle$, where $\mathbf{q}$ is a point in the Brillouin zone and $j=1, 2, \ldots, 9$ is the branch index. The corresponding eigenvalues are $\omega_j^2(\mathbf{q})$.

In SC CdF_2, the conduction band and trap levels have been approximated by Cd^{+2} $5s$-like atomiclike orbitals[5,6] so that the electron may be viewed as hopping between Cd^{+2} sites. If the time τ spent by the electron at any one site is greater than the period of a lattice vibration, then the resulting perturbation of the effective interatomic force constants may produce a resonant lattice mode.[16]

The formulation of the pure lattice problem outlined above is convenient for solution of the local lattice perturbation problem by the Green's-function method. This is so because the appropriate Green's function for the perturbed lattice can be easily constructed from the unperturbed Green's function in terms of the basis states we have introduced. The over-all Green's operator for the pure lattice is defined as

$$\mathbf{G}^0(\omega^2) = (\mathbf{M}\omega^2-\mathbf{\Phi})^{-1}. \tag{10}$$

From Eqs. (8) and (9) this has a spectral decomposition

$$\mathbf{G}^0(\omega^2-i\epsilon) = \mathbf{M}^{-1/2}\sum_{\mathbf{q}j}\frac{|\mathbf{q}j\rangle\langle\mathbf{q}j|}{\omega^2-\omega_j^2(\mathbf{q})-i\epsilon}\mathbf{M}^{-1/2}. \tag{11}$$

The quantity ϵ is small and positive.

[16] Yu A. Izyumov, Advan. Phys. **14**, 569 (1965).

$\mathbf{G}^0$ contains complete information concerning the lattice dynamics of the crystal defined by H_0. For example, noting that

$$\lim_{\epsilon\to 0^+}[\omega^2-\omega_j^2(\mathbf{q})-i\epsilon]^{-1} = \mathrm{PV}[\omega^2-\omega_j^2(\mathbf{q})]^{-1} + i\pi\delta[\omega^2-\omega_j^2(\mathbf{q})], \tag{12}$$

we find the over-all density of states

$$g^0(\omega) = \frac{2\omega}{9N}\sum_{\mathbf{q}j}\delta[\omega^2-\omega_j^2(\mathbf{q})]$$

to be

$$g(\omega) = \frac{2\omega}{9N\pi}\,\mathrm{Im\ Tr}\mathbf{M}^{1/2}\mathbf{G}^0(\omega^2-i0^+)\mathbf{M}^{1/2}. \tag{13}$$

The trace may be carried out in any orthonormal representation. In the above formulae, "PV" stands for "principal value" and "Im" stands for "imaginary part of."

$\mathbf{G}^0(\omega^2)$ also contains within itself the Green's operators describing arbitrary submodes of the lattice. These are simply projections of $\mathbf{G}^0$ onto the appropriate subspace. In particular, let $|A_{1g}\rangle \equiv \sum_{\alpha\kappa l}\xi_\alpha(l,\kappa)|\alpha\kappa l\rangle$ be the normalized A_{1g} symmetry vibration of the XV_8-type complex consisting of a central Cd^{+2} ion at the origin and eight nearest-neighbor F^- ions at the corners of a cube. Such a complex has 27 degrees of freedom and possesses O_h rotational at symmetry. Thus it has vibrational normal modes of A_{1g}, E_g, T_{1g}, A_{2u}, E_u, and T_{2u} symmetry in addition to two modes of T_{2g} symmetry and three modes of T_{1u} symmetry. The state $|A_{1g}\rangle$ consists of in-phase motion of the F^- ions along the body diagonals; there is no motion of the central Cd^{+2}. The coefficients $\xi_\alpha(l,\kappa)$ are chosen to make $|A_{1g}\rangle$ invariant under all operations of the O_h group and are known from elementary group theory.

The distribution of frequencies for this mode is

$$\begin{aligned}g_{A_{1g}}{}^0(\omega) &= \frac{2\omega}{9N\pi}\,\mathrm{Im\ Tr}|A_{1g}\rangle \times\langle A_{1g}|\mathbf{M}^{1/2}\mathbf{G}^0(\omega^2-i0^+)\mathbf{M}^{1/2}\\ &= \frac{2\omega m_F}{9N\pi}\,\mathrm{Im}\langle A_{1g}|\mathbf{G}^0(\omega^2-i0^+)|A_{1g}\rangle.\end{aligned} \tag{14}$$

Evaluation of $\mathrm{Im}\langle A_{1g}|\mathbf{G}^0|A_{1g}\rangle$ is easily carried out since, using Eq. (11) and (12), one need only know $\omega_j(\mathbf{q})$ and $\langle\mathbf{q}j|A_{1g}\rangle = \sum_{\alpha\kappa l}\xi_\alpha(l,\kappa)\langle\mathbf{q}j|\alpha\kappa l\rangle$, or, equivalently, $\omega_j(\mathbf{q})$ and $\langle\mathbf{q}j|\alpha\kappa l\rangle$. Both these latter quantities are known from the diagonalization of the dynamical matrix for the pure crystal. $g_{A_{1g}}{}^0(\omega)$ is given in Fig. 4.

Consider, now, the effect of an electron localized on a Cd^{+2} ion. Neglecting the effect of the trivalent

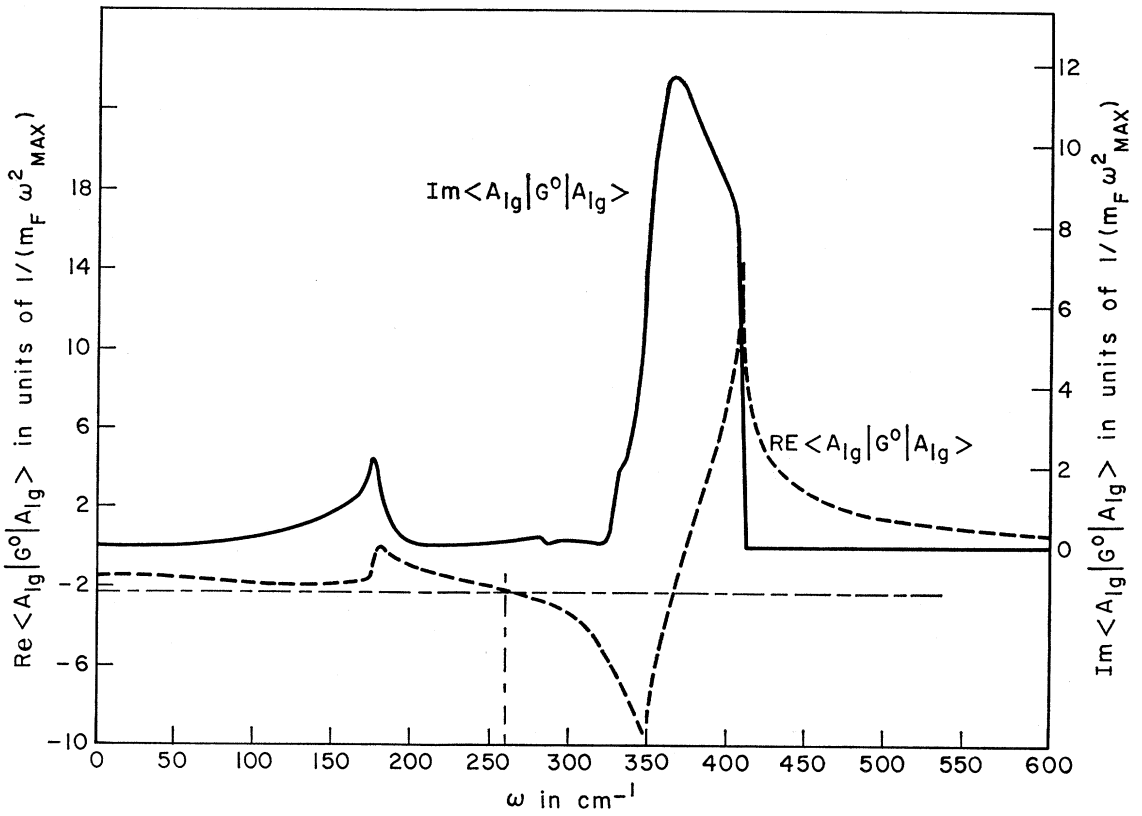

FIG. 13. Real and imaginary parts of the A_{1g} symmetry Green's function calculated by diagonalizing the dynamical matrix at 64 000 points in the Brillouin zone. The horizontal line at $\mathrm{Re}\langle G^0\rangle = -2.25$ is a graphical solution for the resonance condition.

dopant,[17] the resulting changes in the force constants require that the Hamiltonian become

$$H = H_0 + \tfrac{1}{2} \sum_{\alpha\kappa l,\,\alpha'\kappa' l'} \delta\Phi_{\alpha\alpha'}(l\kappa, l'\kappa') u_\alpha(l,\kappa) u_{\alpha'}(l',\kappa') \quad (15)$$

and that the Green's function take the form

$$\begin{aligned} \mathbf{G}(\omega^2) &= (\mathbf{M}\omega^2 - \mathbf{\Phi} - \delta\mathbf{\Phi})^{-1} \\ &= [(\mathbf{M}\omega^2 - \mathbf{\Phi})(1 - \mathbf{G}^0\delta\mathbf{\Phi})]^{-1} \\ &= (1 - \mathbf{G}^0\delta\mathbf{\Phi})^{-1}\mathbf{G}^0. \end{aligned} \quad (16)$$

To evaluate $\mathbf{G}(\omega^2)$ we make the approximation that $\delta\mathbf{\Phi}$ has nonzero matrix elements only within the 27-dimensional subspace γ of $\{|\alpha\kappa l\rangle\}$ defined by the XY_8 complex containing the trapped electron although $\delta\mathbf{\Phi}$ still represents a change in the effective force constants arising both from changes in the long- and short-range forces acting on the ions of the complex.

[17] For the modes centered around the electron, consideration of the additional effects of the impurity make the calculation very cumbersome. Initial considerations, however, suggest that in the nearest-neighbor approximation the effects of the trivalent impurity on the A_{1g} mode of a CdF_8 box centered on a nearest-neighbor Cd site is very small. This is largely because the displacements induced by the trivalent dopant on the two nearest-neighbor fluorines which are also part of the CdF_8 box are almost orthogonal to those induced by the electron. Thus the A_{1g} mode frequency is only perturbed slightly.

The perturbed density of states for the XY_8 A_{1g} symmetry mode is

$$\begin{aligned} g_{A_{1g}}(\omega) &= (2\omega m_F/9N\pi) \\ &\quad \times \mathrm{Im}\langle A_{1g}|\,(1 - \mathbf{G}^0\delta\mathbf{\Phi})^{-1}\mathbf{G}^0|A_{1g}\rangle. \end{aligned} \quad (17)$$

Because $\delta\mathbf{\Phi}$ is localized, the bra vector $\langle A_{1g}|\,(1-\mathbf{G}^0\mathbf{\Phi})^{-1}$ has nonzero scalar products only with ket vectors contained in γ. This can be seen by writing the expansion $(1-\mathbf{G}^0\delta\mathbf{\Phi})^{-1} = 1 + \mathbf{G}^0\delta\mathbf{\Phi} + \mathbf{G}^0\delta\mathbf{\Phi}\mathbf{G}^0\delta\mathbf{\Phi} + \cdots$. Within this subspace we have the completeness relation

$$\sum_{\Omega\beta} |\Omega\beta\rangle\langle\Omega\beta| = 1_\gamma, \quad (18)$$

where $|\Omega\beta\rangle$ is the βth basis state of symmetry Ω in γ and 1_γ is the unit operator in γ. Then, since $\mathbf{G}^0$ has the full symmetry of the lattice,

$$\begin{aligned} &\langle A_{1g}|\,\mathbf{G}\,|A_{1g}\rangle \\ &\quad = \sum_{\Omega\beta} \langle A_{1g}|\,(1-\mathbf{G}^0\delta\mathbf{\Phi})^{-1}|\Omega\beta\rangle\langle\Omega\beta|\,\mathbf{G}^0\,|A_{1g}\rangle \\ &\quad = \langle A_{1g}|\,(1-\mathbf{G}^0\delta\mathbf{\Phi})^{-1}|A_{1g}\rangle\langle A_{1g}|\,\mathbf{G}^0\,|A_{1g}\rangle. \end{aligned} \quad (19)$$

However, $\delta\mathbf{\Phi}$ is diagonal in the $\{|\Omega\beta\rangle\}$ representation, so if we define $\delta\Phi_{A_{1g}} \equiv \langle A_{1g}|\,\delta\mathbf{\Phi}\,|A_{1g}\rangle$ we obtain from

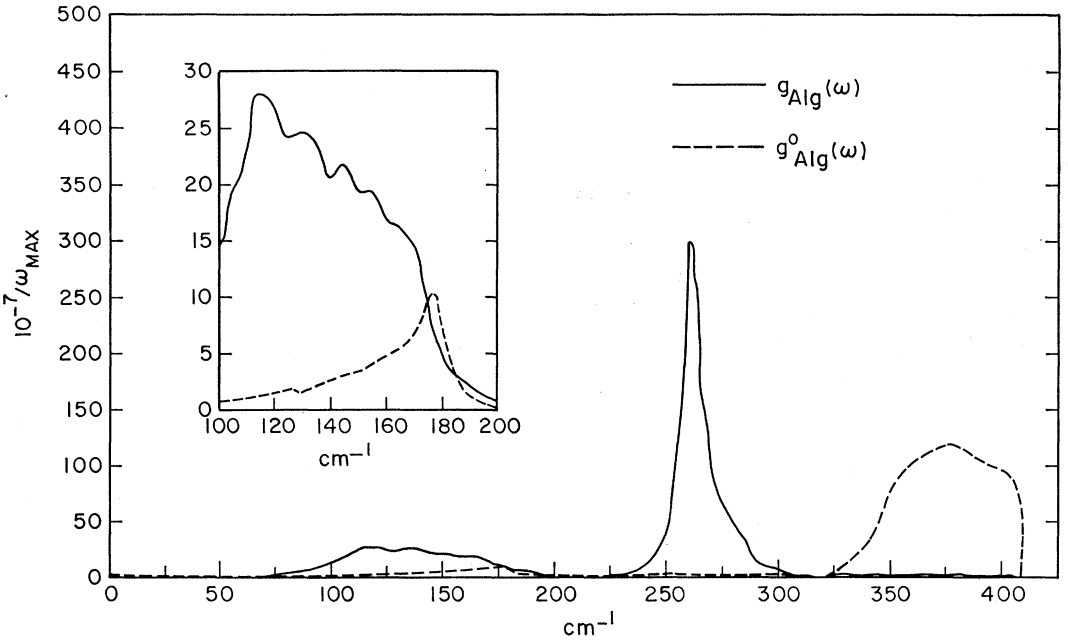

FIG. 14. Perturbed and unperturbed densities of states for the breathing mode of the CdF_8 complex in CdF_2.

Eqs. (17)–(19)

$$g_{A_{1g}}(\omega)=\frac{g_{A_{1g}}{}^0(\omega)}{(1-\mathrm{Re}\langle\mathbf{G}^0\rangle\delta\Phi_{A_{1g}})^2+(\mathrm{Im}\langle\mathbf{G}^0\rangle\delta\Phi_{A_{1g}})^2}, \quad (20)$$

where $\langle\mathbf{G}^0\rangle=\langle A_{1g}|\mathbf{G}^0|A_{1g}\rangle$. $g_{A_{1g}}(\omega)$ exhibits a peak at the frequency where $\langle\mathbf{G}^0(\omega^2)\rangle=1/\delta\Phi_{A_{1g}}$ provided $\mathrm{Im}\langle\mathbf{G}^0\rangle$ is sufficiently small at this frequency. As mentioned, $\mathrm{Im}\langle\mathbf{G}^0\rangle$ is simply calculated directly from the eigenvectors of the dynamical matrix; the real part is then obtained as follows:

$$\begin{aligned}&\mathrm{Re}\langle A_{1g}|\mathbf{G}^0|A_{1g}\rangle\\&=\frac{1}{m_F}\sum_{\mathbf{q}j}\frac{\mathrm{PV}}{\omega^2-\omega_j^2(\mathbf{q})}|\langle A_{1g}|\mathbf{q}j\rangle|^2\\&=\frac{1}{\pi}\mathrm{PV}\int_{-\infty}^{\infty}d\omega'^2\frac{1}{\omega^2-\omega'^2}\\&\quad\times\left\{\frac{\pi}{m_F}\sum_{\mathbf{q}j}|\langle A_{1g}|\mathbf{q}j\rangle|^2\delta[\omega'^2-\omega_j^2(\mathbf{q})]\right\}\\&=\frac{1}{\pi}\mathrm{PV}\int_{-\infty}^{\infty}d\omega'^2\frac{\mathrm{Im}\langle\mathbf{G}^0\rangle}{\omega^2-\omega'^2}.\end{aligned} \quad (21)$$

The real and imaginary parts of $\mathbf{G}^0$ as calculated using the computer program of Lacina[10] are shown in Fig. 13. The horizontal line is chosen to produce a resonance in $g_{A_{1g}}(\omega)$ at $\omega=262$ cm^{-1} and this requires that $\delta\Phi_{A_{1g}}=-84.14\times10^3$ erg/cm^2. The resulting perturbed density of states together with the unperturbed density of states is shown in Fig. 14. The calculated full bandwidth at half-intensity is 11 cm^{-1}. This should be compared to the measured width of 18 cm^{-1}.

In the approximation where one neglects changes in all but nearest-neighbor force constants $\Phi_{F\text{-}F}$ and $\Phi_{Cd\text{-}F}$, diagonalization of $\boldsymbol{\Phi}$ yields

$$\begin{aligned}\Phi_{A_{1g}}&=\Phi_{Cd\text{-}F}+2\Phi_{F\text{-}F}+\Phi',\\\delta\Phi_{A_{1g}}&=\delta\Phi_{Cd\text{-}F}+2\delta\Phi_{F\text{-}F}.\end{aligned} \quad (22)$$

We have included in Φ' all forces arising from the coupling of the central complex to the rest of the crystal, then

$$\frac{\delta\Phi_{A_{1g}}}{\Phi_{A_{1g}}}=\frac{\delta\Phi_{Cd\text{-}F}+2\delta\Phi_{F\text{-}F}}{\Phi_{Cd\text{-}F}+2\Phi_{F\text{-}F}}\left(\frac{1}{1+\Phi'/(\Phi_{Cd\text{-}F}+2\Phi_{F\text{-}F})}\right). \quad (23)$$

The similarity of the unperturbed frequency distribution for the A_{1g} mode to a simple damped harmonic oscillator resonating about 380 cm^{-1} may be evoked to calculate Φ' from the equation

$$m_F\omega_{A_{1g}}{}^2=\{\Phi_{Cd\text{-}F}+2\Phi_{F\text{-}F}\}+\Phi'.$$

If we take values of $\Phi_{Cd\text{-}F}=86\times10^3$ erg/cm^2 and $\Phi_{F\text{-}F}=7.5\times10^3$ erg/cm^2 as determined[9] from pure crystal data, we must have $\Phi'\sim60\times10^3$ erg/cm^2. Of course, Φ' is q dependent and is responsible for the width of the A_{1g} mode. Thus, $\Phi_{A_{1g}}\sim160\times10^3$ erg/cm^2 and we obtain finally

$$\delta\Phi_{A_{1g}}/\Phi_{A_{1g}}\sim-0.5.$$

Note that this result is what would have been obtained by calculating the fractional force constant change

necessary to shift a simple harmonic oscillator from 380 to 260 cm^{-1}.

V. LATTICE-DISTORTION POLARON PROBLEM

In order to make contact with the polaron problem in CdF_2, it is necessary to relate the perturbation $\delta\Phi_{A_{1g}}$ to a lattice department Δr, where Δr is the change in the cadmium to fluorine distance.

From cohesive energy calculations,[9,12] the repulsive potentials appropriate for Cd-F and F-F interactions have the form r^{-N} where $N=7.78$ in the case of Cd-F and $N=10$ in the case of F-F. Thus it is easily shown that

$$\frac{\delta\Phi_{\text{Cd-F}}}{\Phi_{\text{Cd-F}}}=\frac{d^3U/dr^3}{d^2U/dr^2}\Delta r=-(N+2)\frac{\Delta r}{r}=-9.78\frac{\Delta r}{r}.$$

If we ignore the small F-F repulsive contribution and note that the attractive Coulomb term goes as r^{-1}, the condition for equilibrium, $d/dr(U_{\text{attractive}}+U_{\text{repulsive}})=0$, gives

$$\frac{\Delta r}{r}=-\frac{1}{(N-1)}\frac{\delta z_1}{z_1}, \tag{24}$$

where z_1 is the effective charge on the Cd^{+2} site and δz_1 is the change in that charge when the electron is located at the central site. Thus we obtain

$$\frac{\delta\Phi_{A_{1g}}}{\Phi_{A_{1g}}}\cong\frac{(N+2)}{(N-1)}\frac{\delta z_1}{z_1}\left(\frac{1}{1+0.6}\right). \tag{25}$$

If one takes $\delta z_1=-1$ with $z_1=2$ one finds that $\delta\Phi_{A_{1g}}/\Phi_{A_{1g}}=-0.45$, in agreement with the Green's-function calculation. Equation (24) together with the value of $r=2.32$ Å yields

$$\Delta r=0.17\text{ Å}. \tag{26}$$

The displacement of the fluorines away from the Cd^{+2} in response to the presence of the electron is the type of effect responsible for mass enhancement of the conduction electron. The effect of this displacement upon the electron's motion is the central concern of polaron theory. In view of the localization of the distortion suggested by our calculation, a small-polaron model is most appropriate for analyzing the connection between the lattice displacement and the electron's motion.[3,7]

The connection can be made by the analysis of a simple model[18] in which only two neighboring Cd sites are included. The wave function at each site if the electron is at that site is assumed to have the form

$$\Psi_1=\psi_{e1}\psi_1'\psi_2^0,\qquad \Psi_2=\psi_{e2}\psi_1^0\psi_2'. \tag{27}$$

[18] J. Appel, Solid State Phys. **121**, 193 (1968).

Here, ψ_{e1} and ψ_{e2} are electronic wave functions for an electron at Cd sites 1 and 2, respectively. ψ_1' and ψ_1^0 are, respectively, the perturbed and unperturbed A_{1g} phonon harmonic-oscillator wave function at site 1. The perturbed form is appropriate if the electron is at site 1 and the unperturbed one if the electron is at site 2. The reverse, of course, holds for site 2. In the approximation of independent harmonic oscillators centered at the two sites these wave functions are

$$\psi_1^0=\frac{m_F\omega_0^{1/4}}{\pi\hbar}\exp\left(-\frac{m_F\omega_0}{2\hbar}(r_1-r_{10})^2\right),$$
$$\psi_1'=\frac{m_F\omega'^{1/4}}{\pi\hbar}\exp\left(-\frac{m_F\omega'}{2\hbar}(r_1-r_{10}')^2\right), \tag{28}$$

where ω_0 and ω' are the unperturbed and perturbed frequencies of the A_{1g} mode and r_{10} and r_{10}' are the unperturbed and perturbed equilibrium positions of the fluorine atoms, and m_F is the mass of the fluorine atom. The hopping integral between the two sites now becomes

$$\langle\Psi_1|H|\Psi_2\rangle=\langle\psi_{1e}|H|\psi_{2e}\rangle\langle\psi_1'|\psi_1^0\rangle\langle\psi_2'|\psi_2^0\rangle \approx\langle\psi_{e1}|H|\psi_{e2}\rangle\langle\psi_1'|\psi_1^0\rangle^2. \tag{29}$$

The approximate sign is simply to indicate that two of the 16 fluorines actually participate in both modes and also that the effect of the dopant impurity has been neglected. Identifying $\langle\psi_{e1}|H|\psi_{e2}\rangle$ with the band or electronic hopping integral β_b and performing the simple integration using Eq. (28) one finds

$$\langle\Psi_1|H|\Psi_2\rangle=\beta_b\exp[-(m_F\omega'/\hbar)(1-\tfrac{1}{2}\omega'/\bar{\omega})\Delta r^2], \tag{30}$$

where $\Delta r=r_{10}-r_{10}'$ and $\bar{\omega}=\frac{1}{2}(\omega_0+\omega')$. The left-hand side of Eq. (30) is, within our approximation, the polaron hopping integral and using the appropriate values for m_F, ω', $\bar{\omega}$ one finds that

$$\beta_p/\beta_b=e^{-(\Delta r/0.1)^2}. \tag{31}$$

Thus, in the tight-binding band model,

$$m_p/m_b=e^{(10\Delta r)^2}, \tag{32}$$

where m_p and m_b are the polaron and band masses, respectively. Taking $\Delta r=0.17$ Å, this ratio is 18. This result is consistent with the polaron mass of $11m_e$ measured by cyclotron resonance provided that the band mass is reasonably large ($m_b\sim0.6m_e$). In the next section, uv reflection data will be presented from which a band mass of $0.8m_e$ is found.

It is worthwhile to note here that Eq. (32) shows clearly that the polaron mass is a very sensitive function of lattice displacement. In view of the simplicity of the calculation of the displacement, the ratio of 18.0 should only be considered an approximation. The main source of error arises from the assertion in the model calculation that the electron is completely localized for

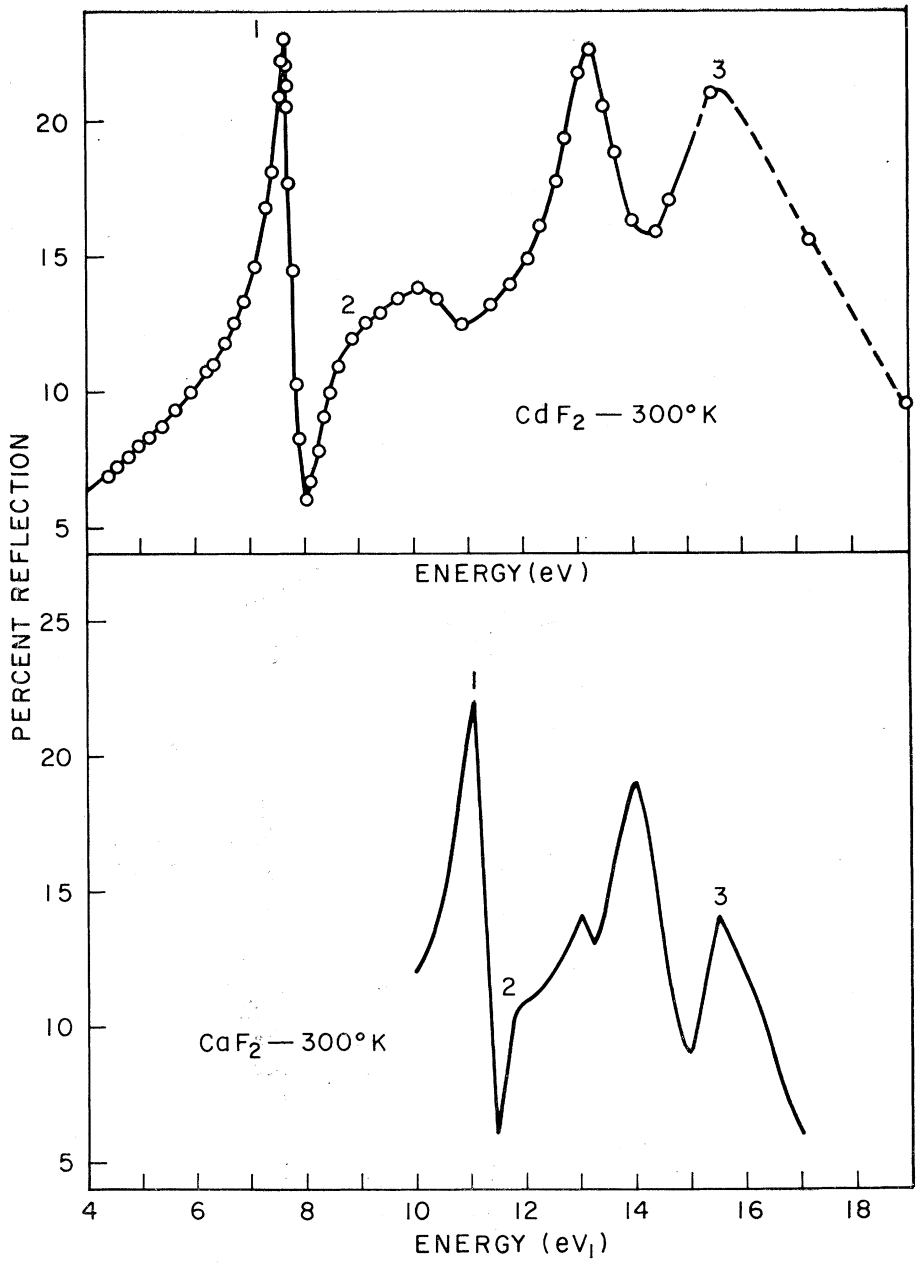

FIG. 15. Ultraviolet reflection spectrum of CdF_2 and CaF_2 at 300°K. The CaF_2 spectrum was obtained from the experiments of Miyata and Tomiki (Ref. 20) and Stephan *et al.* (Ref. 21).

times on the order of the phonon periods and that its perturbing effect is also localized. As the spatial extent of the electronic wave function becomes greater, the lattice displacements near the central site become smaller but the amplitudes die out more slowly as one moves away from the central site.[19] The combined effect of electron delocalization and greater spatial extent of the lattice perturbation is a difficult effect to calculate. We are working in the extreme localization limit for both. This point will be discussed further in Sec. VIII.

VI. ULTRAVIOLET-REFLECTION STUDIES

As can be seen from the analysis of Sec. IV and from other discussions of the polaron problem in CdF_2,[3,4,20] the value of the bare band mass is an important though still unknown parameter. We attempt here to obtain its value from the exciton spectrum of CdF_2.

The experimental results of ultraviolet reflection studies of pure CdF_2 are shown in the top of Fig. 15. It is compared there with the spectrum of CaF_2 mea-

[19] D. M. Eagles, Phys. Rev. **145**, 645 (1966).

[20] T. Miyata and T. Tomiki, J. Phys. Soc. Japan **27**, 957 (1968).

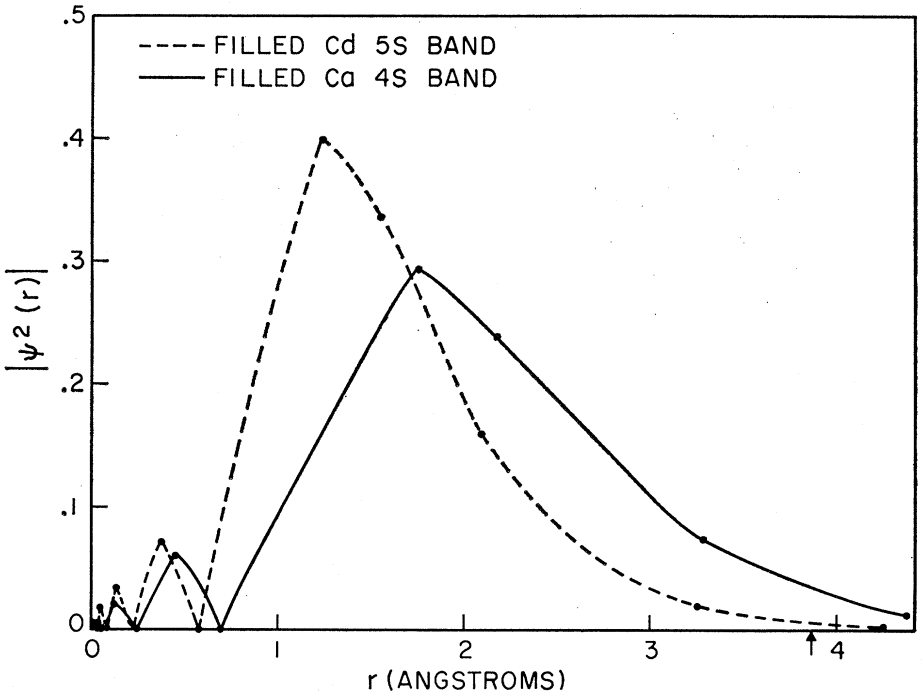

FIG. 16. Electron density of Cd $5s^2$ and Ca $4s^2$ atomic states as a function of distance from the nucleus. The arrow denotes nearest-neighbor metal ion separation in the solid in both CaF_2 and CdF_2.

sured by Miyata and Tomiki[20] and Stephan *et al.*[21] A similar spectrum has also been measured for BaF_2.[20]

There is some experimental difficulty in obtaining uv data on CdF_2. CdF_2, as opposed to the alkaline-earth fluorides, for example, will not cleave. One cannot obtain a natural surface on which to perform uv reflection measurements. Instead, we first followed the procedure of polishing the samples on a hard lap. The resulting uv spectrum only resembled the spectrum shown in the top of Fig. 15 in its major features. Peak 1 was about four times as broad and was shifted to lower energy (6.5 eV). Much of the structure in the higher-energy region was also absent. The broadening and shifting is thought to result from surface damage. It was found that polishing CdF_2 on soft laps resulted in the apparently improved spectrum shown in Fig. 15. The increased sharpness and similarity of the spectrum to that of CaF_2 indicates that the soft lap is preferable, but just how much structure is still obscured due to the surface damage cannot be estimated. An encouraging sign, however, is that peak 1 is sharper in CdF_2 than in CaF_2.

The spectrum of CdF_2 was taken with a McPherson vacuum spectrograph in which deuterium, hydrogen, and argon sources were used for the measurements. A two detector system was utilized so that the incident and reflected intensities were simultaneously measured. Calibration was by use of a freshly coated Al mirror.

The workers who measured the CaF_2 spectrum[20,21] have assigned peak 1 to the $1s$ exciton level and peak 2 to the $2s$ exciton level. From such an interpretation they found a value for the reduced excitonic mass of $0.27m_e$. We give a similar interpretation to peaks 1 and 2 in the CdF_2 spectrum. This assignment results in a binding energy for the exciton of 1.8 eV and the usual hydrogenic excitonic model gives the reduced mass

$$\mu=(E_B/13.6)\epsilon_\infty^2 m_e=0.8m_e,$$

where $\epsilon_\infty=2.4$ is the high-frequency dielectric constant for CdF_2 and E_B is the 1.8-eV binding energy of the exciton. If one assumes an infinite mass for the hole in the narrow fluorine p bands, then the reduced mass becomes the bare electron mass; the reduced mass is therefore the minimum value for the bare electron mass.

There are several difficulties with the interpretation given above. First, it is not clear that peak 2 is the transition to the $2s$ exciton level. Second, it is doubtful that a simple hydrogenic model can explain the $1s$ to $2s$ splitting to better than a factor of 2. The radius of the excitonic orbit is found, in this model, to be 1.6 Å and should be interpreted as the difference between the radius of the electron and the hole. The localized hole should have a radius of 0.64 Å, which gives the fluorine-electron separation as 2.24 Å. This value when compared to the 2.3 Å Cd-F separation indicates that the electron is traveling around the fluorine on the four nearest-neighbor Cd sites. This is typical of excitons in ionic crystals and is thoroughly discussed by Knox.[22]

The relative values of the band edges and effective masses between CaF_2 and CdF_2 do, however, give some support to the validity of the interpretation presented in this section. Since CdF_2 and CaF_2 have the same

[21] G. Stephan, Y. Calrez, J. C. Lemmonier, and S. Robin, Phys. Chem. Solids (to be published).

[22] R. S. Knox, in *Solid State Physics*, edited by F. Seitz and D. Turnbull (Academic Press Inc., New York, 1963) Suppl. 5.

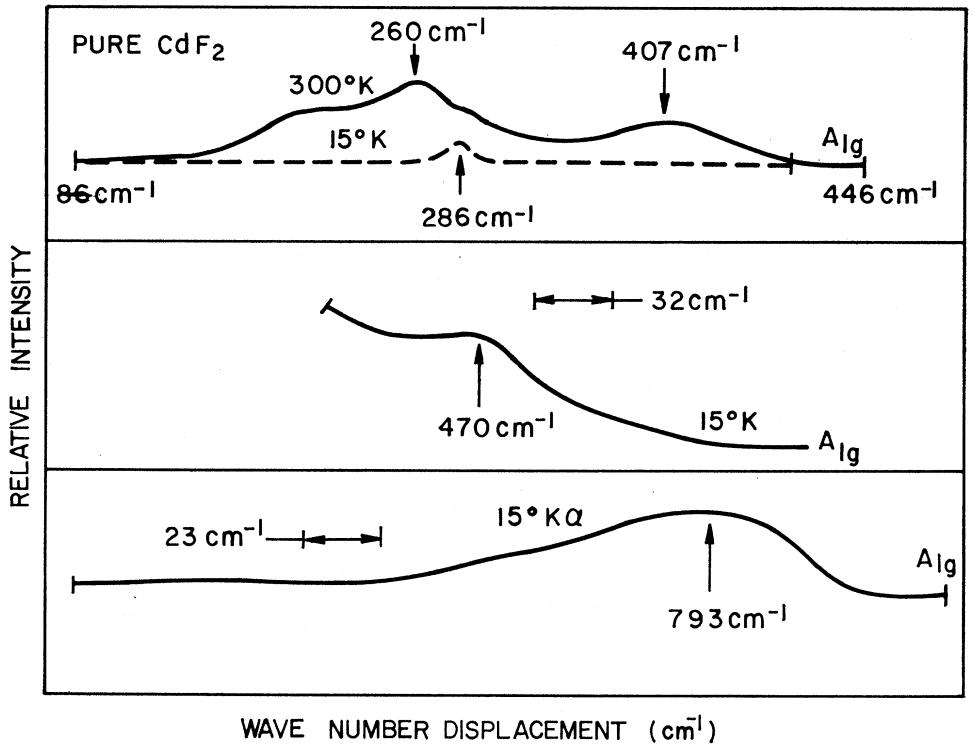

FIG. 17. Two-phonon structure in Raman spectrum of pure CdF_2.

crystal structure, lattice constant, and fluorine ionization energy, the valence-band–conduction-band energy gap should differ mainly because of the differing electron affinities of the Cd^{+2} and Ca^{+2} ions. Similarly, the difference in the electronic band masses in the two systems is a result mainly of the differing spatial extent of the cation wave functions. The electron affinity of Cd^{+2} in the free ionic state is 5 eV greater than Ca^{+2} due to the filled $4d$ shell in Cd which lies only 8.5 eV below the $5s$ shell. In Ca^{+2} there is no filled d shell. In the solid wave function overlap between neighboring double-plus ions reduces the ground-state energy compared to that of the free ion. The degree of this overlap is inversely proportional to the band mass of the electron. Thus, the larger band gap in CdF_2 (by 2.5 eV) is consistent with the band mass calculated in our model. For comparison, the $5s^2$ Cd and $4s^2$ Ca wave function for atomic Cd and Ca are plotted in Fig. 16 from data obtained from Herman and Skillman.[23] The contraction of the Cd wave function relative to Ca is clear from the figure.

VII. DISCUSSION

The model for the trapped and free polaron in CdF_2 which had been previously suggested[5,6] has been further substantiated. The essential features of this model is a heavy mass polaron ($m_p=11m_e$) which is localized. The nature of this localization has been made more quantitative by the observation of the local vibrational mode associated with the presence of the electron. The interpretation of the electron phonon coupling in terms of the A_{1g} mode instead of the usual $\mathbf{q}\cong 0$ LO type distortion is a natural result of localization of the electron. This localization makes other than $\mathbf{q}\cong 0$ optical phonon modes important since the distance parameter which characterizes the extent of the polaron is comparable to a lattice spacing. The large density of states of the A_{1g} mode around 380 cm^{-1} can be thought of as arising from symmetric combinations of nonzero-$\mathbf{q}$ LO optical modes (i.e., they are the only normal modes which have any density of states in the 360–410-cm^{-1} region). Of course, in the case of complete localization, one could expect the coupling to be independent of $\mathbf{q}$. In the simple model calculation performed in Sec. IV, something approaching complete localization was assumed and thus the distortion was only at the nearest-neighbor sites. To the extent that the electronic wave function is nonlocalized, the displacements are no longer mainly on the eight nearest-neighbor sites, and thus the coupling will be $\mathbf{q}$-dependent. In the limit of a highly nonlocal electronic wave function, $\mathbf{q}=0$ coupling predominates and the large-polaron model is expected to apply.

Thus, the central assumption of the small-polaron model used in this paper concerns the question of localization. In our two-site model it would seem that a sufficient condition for the phonons to follow adiabatically the motion of the electron would be if $2\beta_p<\hbar\omega_0$.

[23] F. Herman and S. Skillman, *Atomic Structure Calculations* (Prentice-Hall, Inc., Englewood Cliffs, N. J., 1963).

TABLE II. Second-order Raman structure. Difference and sum stand, respectively, for two-phonon difference and sum processes. R—Raman branch, A—acoustic branch, O—optic branch. X and L are the (100) and (111) Brillouin-zone symmetry points.

Energy (cm^{-1})	Nature	Symmetry	Source
260–260	Broad, difference	A_{1g}	$R(L)-TA(L)$
260	Peak, difference	A_{1g}	$R(L)-TA(L)$
280	Peak, sum	A_{1g}	$2TA(X)$
470	Peak, sum	A_{1g}	$TO(L)+LA(L)$
803	Broad, sum	A_{1g}	$2LO(X)$
407	Peak	A_{1g}	LO

However, in the solid there are more nearest neighbors to which the electron can hop, and thus its lifetime at one site is reduced. The condition for localization would then be roughly that $Z\beta_p < \hbar\omega_0$, where Z is the number of nearest neighbors. Near a trivalent dopant, $Z=4$ and the inequality just holds. Away from the dopant where $Z=12$, the inequality would not hold for the numbers used in our calculation—$\beta_p \sim 0.01$ eV, $\hbar\omega_0 \sim 0.05$ eV. For such a situation the wave function given in Eq. (27) and the hopping integral given in Eq. (29) would no longer be correct. A self-consistent treatment of the electron and phonon systems is required. The present lack of such a treatment is at the core of the difficulty in understanding the nature of the intermediate-size polaron. A strong suggestion that an intermediate treatment is required is evident when one compares the polaron to band mass enhancements predicted by the large-polaron model,[6,17] the small-polaron model calculated here, and the measured enhancement obtained from the ratio of the polaron to excitonic mass. The values are 8 for the large polaron and 18 for the small polaron, while the measured ratio is 13.7. The implication is clear; we suggest that semiconducting CdF_2 may be a good testing ground for intermediate-polaron theories.

Finally, we temper our conclusions with a word of caution. In each of the experiments described in this paper and those in previous works[4–6] there are features whose interpretations cannot be conclusively stated. Had they been interpreted differently, we would have to alter the physical interpretation of some phenomena reported in this paper. For example, in the uv studies the question arises as to whether peak 2 is really the $n=2$ transition of a hydrogeniclike exciton and, if it is, what is the exact meaning of the mass deduced; the concept of a band mass over such a small physical region is somewhat tenuous. The assumption of an infinite mass for the hole may also be incorrect. In the Raman studies there is the possibility that both the 180-cm^{-1} and 262-cm^{-1} lines have an origin other than that which has been assigned to them. For example, the 180-cm^{-1} peak could be a phononlike transition possibly arising from the small density-of-states peak at 180 cm^{-1} which is present in the unperturbed A_{1g} density of states (Fig. 4). The reason for the failure to see the larger A_{1g} phonon density at 380 cm^{-1} would not be clear in such a model. The disappearance of the observed peak at 100°K would also be unexplained. The 262-cm^{-1} line would seem to have to be a local mode due to the lack of any A_{1g} density of states in that region in pure CdF_2. However, its origin could be different than that presented here and might arise from a mode centered around the trivalent impurity. Initial considerations, however, suggest that the effect of the extra positive charge in the trivalent dopant would be to increase the force constants and thus increase the frequency of the A_{1g} mode above its value in the pure crystal.

Even considering all these alternatives we are unable to formulate an alternative model which can successfully explain the results.

If, however, the interpretation presented in this paper does apply at least as far as its general physical model is concerned, then it will be the first example of a polaron in which the effects of electron-phonon coupling on both the electron and phonon properties of a system have been experimentally connected.

ACKNOWLEDGMENTS

We are indebted to Professor P. S. Pershan for many valuable discussions and for his reading of the manuscript. We thank P. Fleury in whose laboratory the Raman measurements were carried out, and S. K. Kurtz in whose laboratory the uv reflection data were taken. We give special thanks to B. Lacina, who kindly loaned us his computer programs for the fluorite lattice and aided us in their implementation.

APPENDIX: TWO-PHONON RAMAN STRUCTURE

In addition to the allowed Raman transition at 322 cm^{-1}, considerable two-phonon structure was observed. All the structure had A_{1g} symmetry and was observed with both the 4880 and 5145 Å excitation frequencies. This structure is shown in Fig. 17, where the results at several temperatures are given to show which peaks are at two-phonon sum frequencies and which are at two-phonon difference frequencies. The results are collected in Table II. The last column is deduced from the calculated dispersion diagrams (Fig. 2) and the selection rules for two-phonon Raman-active processes which allow $\mathbf{q}\neq 0$ phonons to participate. The identifications are considered only tentative. A more exact identification can be made by a calculation of the two-phonon A_{1g} density of states.[24] Though the 407-cm^{-1} line was absent at 15°K, upon heating the sample it had reappeared by 30°K. There was also an indication of a line at 224 cm^{-1} at low temperatures. The existence in the Raman spectrum of signals at 224 cm^{-1} and 407 cm^{-1} which correspond to the TO and LO frequencies of pure lattice may be coincidental or may result from the presence of impurities or strains both of which partially could destroy the parity selection rules.

[24] A. M. Karo and J. Hardy, Phys. Rev. **141**, 696 (1966).